ENSO at 6ka and 21ka from ocean–atmosphere coupled model simulations

W. Zheng · P. Braconnot · E. Guilyardi · U. Merkel · Y. Yu

Abstract We analyze how the characteristics of El Niño-Southern Oscillation (ENSO) are changed in coupled ocean–atmosphere simulations of the mid-Holocene (MH) and the Last Glacial Maximum (LGM) performed as part of the Paleoclimate Modeling Intercomparison Project phase 2 (PMIP2). Comparison of the model results with present day observations show that most of the models reproduce the large scale features of the tropical Pacific like the SST gradient, the mean SST and the mean seasonal cycles. All models simulate the ENSO variability, although with different skill. Our analyses show that several relationships between El Niño amplitude and the mean state across the different control simulations are still valid for simulations of the MH and the LGM. Results for the MH show a consistent El Niño amplitude decrease. It can be related to the large scale atmospheric circulation changes. While the Northern Hemisphere receives more insolation during the summer time, the Asian summer monsoon system is strengthened which leads to the enhancement of the Walker circulation. Easterlies prevailing over the central eastern Pacific induce an equatorial upwelling that damps the El Niño development. Results are less conclusive for 21ka. Large scale dynamic competes with changes in local heat fluxes, so that model shows a wide range of responses, as it is the case in future climate projections.

W. Zheng (✉) · Y. Yu
State Key Laboratory of Numerical Modeling for Atmospheric Sciences and Geophysical Fluid Dynamics,
Institute of Atmospheric Physics,
Chinese Academy of Sciences, Beijing 100029, China
e-mail: zhengwp@mail.iap.ac.cn

W. Zheng · P. Braconnot
Laboratoire des Sciences du Climat et de l'Environnement
(IPSL/LSCE), Gif-sur-Yvette, 91191 Paris, France

E. Guilyardi
Laboratoire d'Océanographie et du Climat:
Expérimentation et Approches Numériques (IPSL/LOCEAN),
Jussieu, 75252 Paris, France

E. Guilyardi
Walker Institute, University of Reading, Reading RG6 6BB, UK

U. Merkel
FB5 Geosciences, Department of Geosystem Modeling,
University of Bremen, 28359 Bremen, Germany

W. Zheng
Graduate University of the Chinese Academy of Sciences,
Beijing 100039, China

1 Introduction

The El Niño-Southern Oscillation (ENSO), originating from the tropical Pacific, is the strongest mode of climate variability on interannual timescales. It involves oceanic dynamics (Rassmusson and Carpenter 1982; Battisti and Hirst 1989; Jin 1997) as well as large-scale atmospheric changes (Bjerknes 1969; Gill 1982). Because of its dramatic impacts on the global climate that directly affect the human societies, there is a great need to further understand ENSO. In the last two decades, theoretical studies and model simulations of ENSO have progressed rapidly (Wang and Picaut 2004). Analyses of several ENSO events suggest that the mechanisms that drive the basic state and the seasonal cycle in the tropical Pacific, such as the Gill's response (Gill 1982) and the Bjerknes feedbacks, do operate during El Niño events (Chang 1996). But the intensity and frequency of ENSO and the link between ENSO variability and the mean state of the tropical Pacific are not yet completely

understood. This remains an important issue for future climate change. In particular, the specific roles of the mean state and seasonal cycle of the tropical Pacific in influencing ENSO characteristics are not yet fully understood. In that sense, studying paleoclimates that exhibit a mean state or seasonal cycle significantly different from today's can further help to elucidate these interactions.

Indeed, substantial changes in ENSO variability at different time scales have been identified from past climate data (Rodbell et al. 1999). Natural archives such as corals, ice cores and lake sediments have suggested that the intensity and frequency of ENSO were decreased during the MH (6ka BP) compared to modern climate (see Cole 2001 for a review). Several studies have suggested that these changes in ENSO characteristics can be related to the mean climate of the tropical Pacific. Liu et al. (2000), for example, attributed the MH ENSO suppression to the enhanced Asian monsoon circulation and to a weaker teleconnection with the southern Pacific. Clement et al. (2000) discussed why the western Pacific warms more than the eastern Pacific in response to the uniform MH summer heating by increased solar radiation. They argued that the corresponding zonal sea surface temperature (SST) gradient would sustain anomalous easterlies that damp the El Niño development. For the LGM (21ka BP) paleo-temperature reconstructions for the tropical Pacific are ambivalent. While some studies (Lea et al. 2000) report a larger cooling in the cold tongue than in the warm pool region, others (Koutavas et al. 2002) show a pattern more consistent with a peak El Niño-like mean state. Model simulations also lead to different conclusions. Otto-Bliesner et al. (2003) and An et al. (2004) show stronger ENSO activity for the LGM and a weakening of the tropical Pacific zonal SST gradient, wind stress, upwelling and a sharpening of the tropical thermocline. Peltier (2004), using a version of the CCSM model slightly different than Otto-Bliesner et al. (2003), came to opposite conclusions. There is thus still a need to better understand the ENSO behavior for this cold climate. This analysis of past climates provides different sources of El Niño variations that can help to further understand the ENSO in response to CO_2 forcing in the future and the evolution of the zonal SST gradient in the equatorial Pacific.

As part of the second phase of the Paleoclimate Modeling Intercomparison Project (PMIP, Harrison et al. 2002) several modeling groups produced coordinated simulations of the MH and the LGM. The MH experiment is designed to examine the climate response to a change in the seasonal and latitudinal distribution of incoming solar radiation (insolation) caused by known changes in orbital forcing, whereas the LGM experiment is designed to examine the climate response to the presence of large ice sheets, lower sea level and lower greenhouse gas (GHG) concentrations

(Braconnot et al. 2007a). We use in the following these sets of simulations to investigate how the ENSO characteristics are altered for these two climates driven by different forcing. We address the following questions: Are PMIP2 coupled simulations able to reproduce key ENSO characteristics in the tropical Pacific? Do the PMIP2 simulations produce consistent ENSO changes for the MH and LGM climates? Can we highlight key mechanisms for these changes? We build on the study of Guilyardi (2006, hereinafter referred to as G06) who considers changes in ENSO in future climate projections using the CMIP3 multi-model database where future climate projections made for the fourth IPCC assessment have been gathered. The reason is that the diagnostics developed by G06 consider the relationship between the interannual variability in the tropical Pacific and the mean tropical climate as well as the mean seasonal cycle. These diagnostics seem thus well suited to be used in our paleoclimate study, since the MH is characterized by an amplification of the mean seasonal cycle of temperature in Northern Hemisphere (NH) and the LGM by a massive annual mean cooling.

The paper is organized as follows: PMIP2 experiments and model results of the tropical Pacific mean climate are briefly described in Sect. 2. Section 3 analyses the El Niño characteristics of all three scenarios available, including key characteristics such as the amplitude and frequency of El Niño. The possible mechanisms for changes in El Niño properties are discussed in Sect. 4. Conclusions are presented in Sect. 5.

2 Models and PMIP2 experiments

2.1 Experimental design

In contrast to PMIP1, simulations using fully coupled ocean–atmosphere general circulation models have become available in PMIP2. All PMIP2 participants had to follow the PMIP2 protocol (http://www.lsce.cea.fr/pmip2) in setting up the simulations (see Braconnot et al. 2007a for a detailed description).

The control simulation (0ka) corresponds to a pre-industrial climate. The orbital parameters, the ice sheets and the topography are set to present day values and the GHG concentrations (CO_2, CH_4, N_2O, CFCs and O_3) are prescribed to values for 1750 AD.

The MH simulation (6ka) is forced with the same continental ice sheets and topography as in the control simulation. The same atmospheric trace gases as in the control simulation are prescribed except for CH_4 which is reduced from 760 to 650 ppb. Insolation is the major difference compared to the control simulation. The orbital parameters are prescribed from Berger (1978). They lead to

an increased seasonal cycle of insolation in the NH and a decreased seasonal cycle in the Southern Hemisphere (SH).

For the LGM (21ka), the presence of large ice sheets in the NH and lower trace gas concentrations represent the key differences with present day climate. The LGM simulation is forced with the ICE-5G ice sheet reconstruction (Peltier 2004). The land–sea mask and the topography are also changed to be consistent with the ice sheets. Atmospheric GHG concentrations are lowered according to LGM reconstructions. River routing and ice sheet melting are also considered in some of the simulations. Orbital parameters do not differ much from the control simulations, so that insolation is nearly as it is today. Each modeling group adopted its own strategy to bring the ocean into a cold state.

Results of the last 100–200 years of each simulation are archived in the PMIP2 database (http://www-lsce.cea.fr/pmip2). In our study, we consider seven models for which monthly data have been submitted to the PMIP2 database. A list with information on model resolution and model references is given in Table 1. The coupling procedure and the spin-up strategy are model dependent and described in the references of the models (Table 1). All simulations were run long enough to be representative of an equilibrium climate. However, Braconnot et al. (2007a) show that some of the models exhibit a residual long term climate drift. This drift is negligible in the tropical regions. All models listed in Table 1 were used to run the MH experiments, whereas LGM climate was only provided for four of them. Except for CCSM3, 100 years of monthly values are available to analyze interannual variability for each period. For some of the modeling groups (FGAOLS-1.0g, IPSL-CM4 and MIROC3.2) the model version used to perform PMIP2 simulations is exactly the same as the one used to perform future climate projection following the scenarios recommended for the fourth IPCC report.

To assess model performance for the control climate (pre-industrial simulation), we use SSTs from the HadISST1.1 dataset (Rayner et al. 2003) for the period 1870–2000 and SSTs and wind stress from NCEP reanalysis data (Kistler et al. 2001) for the period 1948–2001.

2.2 Simulated mean climate of the tropical Pacific

The annual mean SST simulated by each coupled model for the control climate is displayed in Fig. 1 together with the corresponding modern observations (see also Braconnot et al. 2007a, b for an overview of the mean climate simulated by PMIP2). Most of the models capture the large scale distribution of the annual mean SST, such as the warm pool region in the western Pacific and the equatorial cold tongue in the eastern Pacific. As the GHG concentrations are set to pre-industrial values for the control simulations, the simulated SSTs should be lower than in modern observations. Indeed, most models simulate cooler SSTs in the warm pool area and in subtropical regions. The common biases of non-flux-corrected GCMs (Latif et al. 2001) are present in most of the PMIP2 simulations. The equatorial cold tongue penetrates far too west into the western Pacific which leads to a westward shift and an erosion of the warm pool. Warmer than observed SSTs are found in the eastern Pacific around 8°S, which shows the signature of the classical "double ITCZ" bias (not shown). Table 2 summarizes several characteristics of the mean climate such as the Niño 3 (5°S–5°N; 150°W–90°W) SST and the Niño 4 (5°S–5°N; 160°E–150°W) zonal wind stress. As already noted, most models tend to have a cooler Niño3 SST than observations with two extreme cases (more than 2°C cooler, FOAM and MRI-CGCM2.3.4nfa) while IPSL-CM4 simulates a warmer Niño3 SST than the observations. The cooler SSTs are associated with the westward penetration of the cold tongue (Fig. 1) which can be related to the too strong wind stress simulated over the Niño4 region (Table 2). Four models produce a wind stress which is too large by about 30% (FOAM, MIROC3.2 and

Table 1 Coupled models used in this study, including model resolution, number of years archived in the PMIP2 database, and model references

Model	Institution	Atmosphere resolution	Ocean resolution	Length of simulations			Reference
				0ka	6ka	21ka	
CCSM3	NCAR (USA)	T42L18	1.125° × 0.27°L40	50	50	50	Collins et al. (2006)
FGOALS-1.0g	LASG/IAP (China)	2.8125° × 3°L26	1° × 1°L33	100	100	100	Yu et al. (2002, 2004)
FOAM	University of Bristol (UK)	R15L18	2.8° × 1.4°L24	100	100	N/A	Jacob et al. (2001)
IPSL-CM4	IPSL (France)	3.75° × 2.5°L19	2° × 1°L31	100	100	100	Marti et al. (2005)
MIROC3.2	CCSR/NIES/FRCGC (Japan)	T42L20	1.4° × 0.5°L43	100	100	100	K-1 Model Developers (2004)
MRI-CGCM2.3.4fa	MRI (Japan)	T42L30	2.5° × 0.5°L23	100	100	N/A	Yukimoto and Noda (2002)
MRI-CGCM2.3.4nfa	MRI (Japan)	T42L30	2.5° × 0.5°L23	100	100	N/A	Yukimoto and Noda (2002)

Fig. 1 Annual mean SST for
the control simulations (0ka) as
observed from the NCEP data
and simulated by the different
models. Isolines are plotted
every °C. The average of years
1948 to 2001 is considered for
NCEP
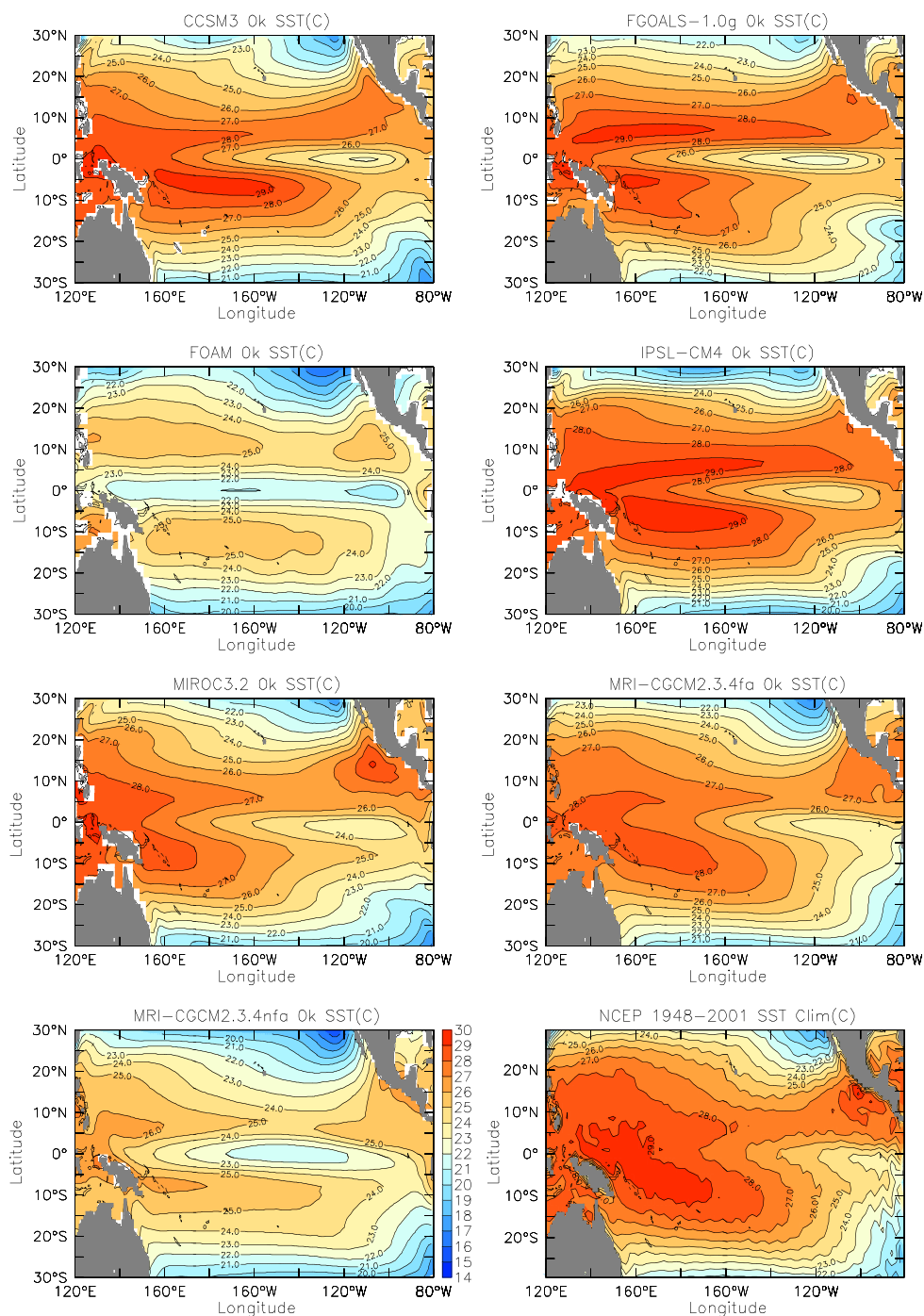
two MRIs). The values simulated by the other three models
are in better agreement with observations (CCSM3, FGO-
ALS-1.0g and IPSL-CM4).

2.3 Changes in the mean climate characteristics for MH and LGM

The changes of the annual mean SST compared to 0ka are
shown for MH in Fig. 2 and LGM in Fig. 3 respectively.

For the MH, the most striking feature is a stronger cooling
at low latitudes and a minor cooling (or warming) in the
subtropical regions of the SH and near the western coast of
North America (Fig. 2). Two models (FGOALS-1.0g and
FOAM) show a significant cooling center in the central and
eastern Pacific and a warming in the western Pacific while
another model (MRI-CGCM2.3.4nfa) shows a similar
pattern but of a SST cooling everywhere and cooler SST in
the central and eastern Pacific (Fig. 2). The cooling in the
tropical region is a direct response to annual mean

Table 2 Main El Niño features for the different models and the observations

Model	Code	Amplitude	Period (year)	SST (°C) Niño3	TAUX (Pa) Niño4	Amplitude change (%)	
						6ka	21ka
Observed	OBS	0.80 ± 0.04	3.6/5.4	25.70 ± 0.06	–0.029 ± 0.001		
CCSM3	A	0.94 ± 0.06	2.0	25.24 ± 0.09	–0.033 ± 0.001	*–18.6*	*–35.8*
FGOALS–1.0g*	B	1.91 ± 0.11	4.5	25.19 ± 0.16	–0.033 ± 0.001	*–14.6*	–4.1
FOAM	C	0.76 ± 0.03	4.1	22.27 ± 0.05	–0.040 ± 0.001	*–11.6*	
IPSL-CM4*	D	1.03 ± 0.04	2.8	26.36 ± 0.08	–0.026 ± 0.000	–2.9	–1.3
MIROC3.2*	E	0.51 ± 0.03	4.3	24.85 ± 0.04	–0.041 ± 0.000	*–22.5*	*12.2*
MRI-CGCM2.3.4fa	F	0.65 ± 0.03	2.4	24.92 ± 0.05	–0.040 ± 0.001	3.3	
MRI-CGCM2.3.4nfa	G	0.63 ± 0.04	2.3	23.14 ± 0.05	–0.043 ± 0.001	*–12.9*	

The El Niño amplitude changes of 6ka and 21ka (when compared to 0ka) are shown in the last two columns. The El Niño amplitude is defined as the standard deviation of monthly SST anomaly in the Niño3 region. Errors were estimated with a moving block bootstrap to account for serial correlation (windows: El Niño period of Fig. 1 for standard deviation and 10 months for means). The amplitude change values italicized are significant at the 5% level by F test. The model with an asterisk means that the model version is the same as in CMIP3

insolation, mostly due to winter and spring conditions (Braconnot et al. 2000; Liu et al. 2003). Indeed, the reduction of insolation reaches about 20 W/m^2 from January to March within the tropics (30°N–30°S). Then the insolation change is larger in the NH than in the SH where the increase in insolation becomes significant only in August. The amplitude of SST change in the NH is larger than that in the SH, which also reflects the amplification of the seasonal cycle of insolation in the NH and its damping in the SH.

For the LGM, all models simulate a systematic cooling of the SST in response to the reduction of the GHG concentrations and to the presence of ice sheets in the NH (Fig. 3). Studies suggest that the GHG concentrations provide the larger contribution to the response and may account for about half of the simulated tropical cooling (Shin et al. 2003; Liu et al. 2005). The cooling is mainly centered in the equatorial region and along the western coast of North America. Two models (IPSL-CM4 and MIROC3.2) show a stronger response in the eastern Pacific than in the western Pacific. These simulations compare reasonably well with the results by Otto-Bliesner et al. (B.L. Otto-Bliesner, R. Schneider, E.C. Brady, M. Kucera M, A. Abe-Ouchi, P. Braconnot, M. Crucifix, C. Hewitt, M. Kageyama, O. Marti, A. Paul, A. Rosell-Melé, S.L. Weber, M. Weinelt, Y. Yu: A comparison of PMIP2 model simulations and the MARGO proxy reconstruction for tropical sea surface temperatures at Last Glacial Maximum, in preparation).

We further examine the seasonal cycle of SST in the Niño3 region for the three experiments (Fig. 4). Most models simulate properly the phase of the seasonal cycle of the SST compared to observations, except for FGOALS-1.0g which has a shift of about 6 months and FOAM which tends to have a semi-annual cycle in the Niño3 region (Fig. 4a). Compared to control simulations, although the

seasonal cycle of NH is increased for MH, all models produce a consistent decrease of the amplitude of the Niño3 SST seasonal variation but little phase change of the seasonal cycle (Fig. 4b), which is mainly due to the weakened seasonal signal from the Southern hemisphere. Also the southward shift of the ITCZ in the region of the Panama isthmus discussed in Braconnot et al. (2007b) reduces the northward component of the wind stress along near the equator in the eastern pacific, and certainly contributes to damp the amplitude of the seasonal upwelling (Braconnot et al. 2007c)

The changes are less consistent between different models for the LGM simulations. The phase of the seasonal cycle is mostly as it is today, but the SST amplitude changes are model dependent. Two models (CCSM3 and MIROC.2) show a slight tendency to enhance the amplitude of the seasonal cycle, whereas the other two produce no change (Fig. 4c). Even though all models simulate a southward shift of the ITCZ like for 6ka in the region of the Panama Isthmus (Braconnot et al. 2007b), the reduction of the wind stress is effective over all the Pacific ocean in the southern hemisphere (not show). Therefore large scale heat fluxes and dynamics may have a larger impact on the changes in the amplitude of the equatorial upwelling than the local dynamics along the eastern part of the tropical Pacific.

3 ENSO characteristics

The Niño3 index is a classical indicator of ENSO variability. Large variability of tropical Pacific SSTs in the MH and LGM simulations is also found in the Niño3 region. G06 uses Niño3 index to analyze the results of 23 CGCMs that were used to perform pre-industrial simulations and

Fig. 2 Simulated changes in annual mean SST for the MH (6ka). Isolines are plotted every 0.1°C
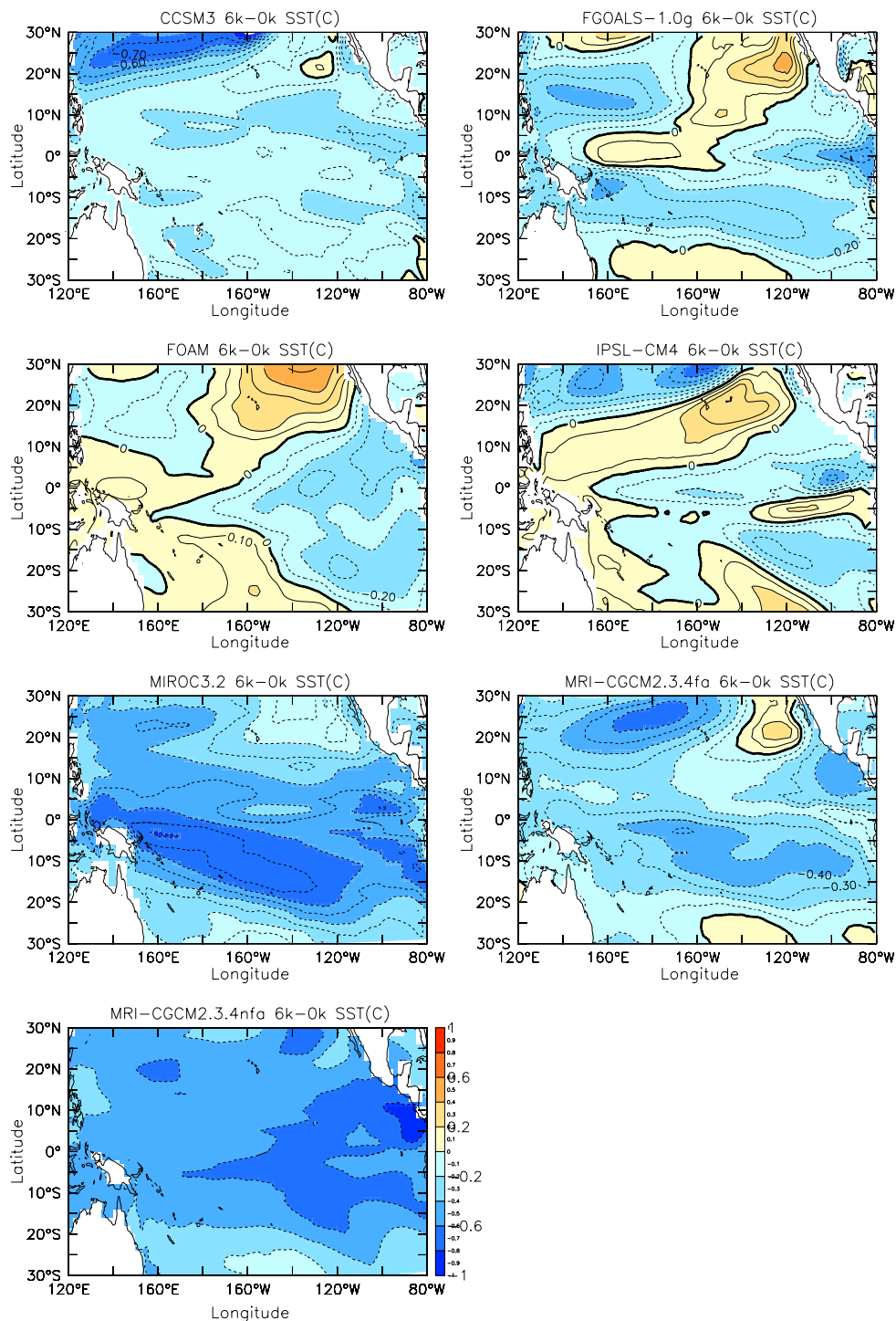
future climate projections in which the CO_2 concentration is increased by 1% per year. Several relationships between this index and the mean state and the seasonal cycle were found amongst the models that follow quite well the conclusions of theoretical works. Of particular interest here is the fact that G06 shows an inverse relationship between the ENSO amplitude and the wind stress in the tropical Pacific. The approach of G06 is well suited to study the mean state—seasonal cycle—ENSO relationships in the PMIP2 simulations. In the following we first discuss these relationships for the control simulations, and then analyze how they change for the MH and LGM.
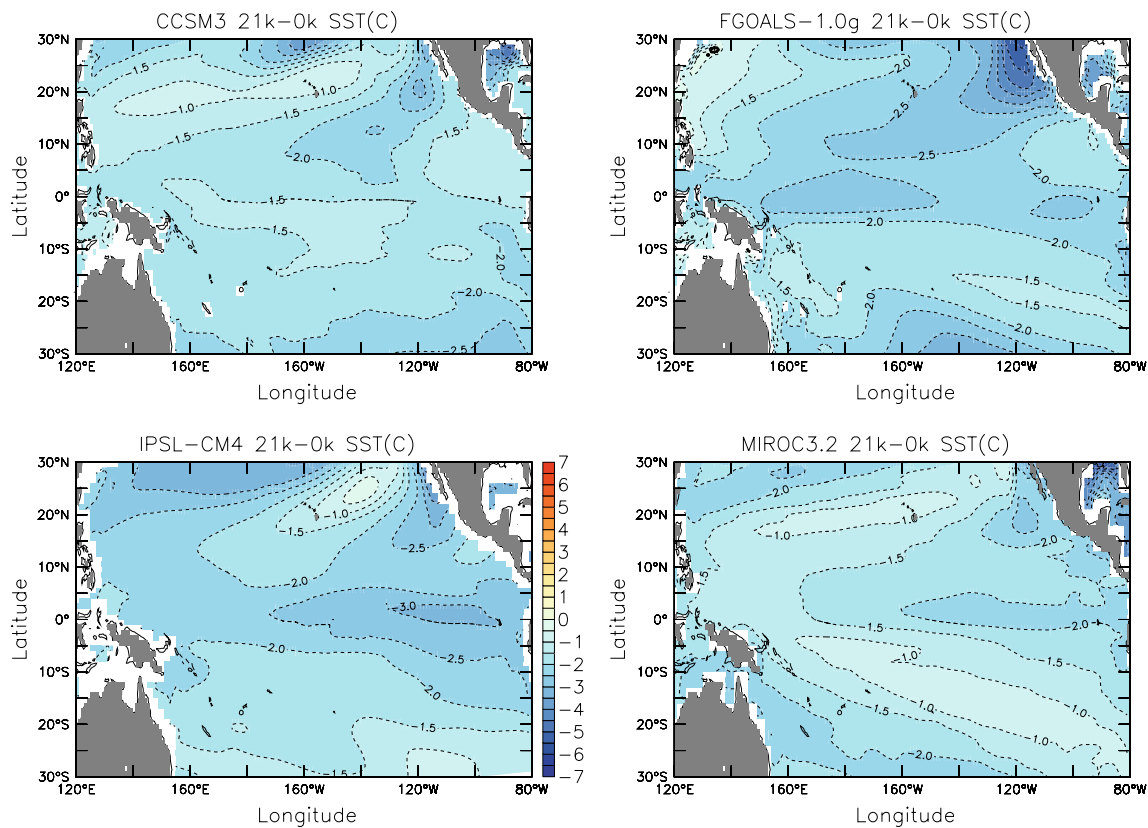
Fig. 3 Same as Fig. 2 but for the LGM (21ka). Isolines are plotted every 0.5°C

3.1 ENSO characteristics of 0ka simulations

We characterize ENSO by using the amplitude of El Niño events estimated as the standard deviation of the Niño3 index and by the statistically significant frequency at the 5% level of confidence estimated by a spectral analysis. Compared to the observations, Table 2 shows that the El Niño amplitudes of the control simulation fall into three categories: (1) those with a weaker amplitude than the observations (MIROC3.2 and MRI-CGCM2.3.4nfa); (2) those within ±20% of the observation (CCSM3, FOAM and MRI-CGCM2.3.4fa); and (3) those with a larger- to much larger-than-observed variability (FGOALS-1.0g and IPSL-CM4). The spectral analysis of the HadISST1.1 data from 1,870 to 2,000 shows two peaks around 3.6 and 5.4 years for the observations (Fig. 5; Table 2). The CCSM3, IPSL-CM4 and the two MRIs simulate a higher frequency than observed. Moreover, these models also exhibit too regular events as shown by a single peak concentrating all the spectral energy (Fig. 5). The other three models show broadly correct dominant frequency about 4 years (FGO-ALS-1.0g, FOAM and MIROC3.2), yet they also exhibit too regular events (Fig. 5).

As shown in G06 for the CMIP3 simulations, models that simulate the larger trade winds in the Niño 4 region

also exhibit lower SST in the Niño 3 region. Following G06, the relationship between the mean Niño4 wind stress and mean Niño3 SST in the PMIP2 simulations also shows the robust correlation between increased SST in the east Pacific and decreased equatorial trade winds (Fig. 6a). Except for FGOALS-1.0g, the relationship between the amplitude of SST anomalies and wind stress in the Niño4 region is also found, so that models with a weaker El Niño also produce larger trade winds (Fig. 6b)

The seasonal phase lock (SPL) is defined in G06 as the annual amplitude of the monthly stratified standard deviation of the Niño3 SST. The El Niño amplitude has an almost linear relationship with the SPL index (Fig. 6c) except for FGOALS-1.0g, which indicates the key role of a seasonal relaxation of the winds to allow large El Niño events development (Fedorov and Philander 2001). A weak SPL means that the seasonal cycle does not offer a relaxation time for El Niño to develop whereas a large SPL will offer opportunities for El Niño development. Three models (CCSM3, FGOALS-1.0g, and MRI-CGCM2.3.4nfa) have a SPL value close to observed.

We further quantify the relationship between the seasonal cycle and the El Niño amplitude, by computing the seasonal cycle relative strength (SCRS). The SCRS is defined as the ratio of the energy between the combined
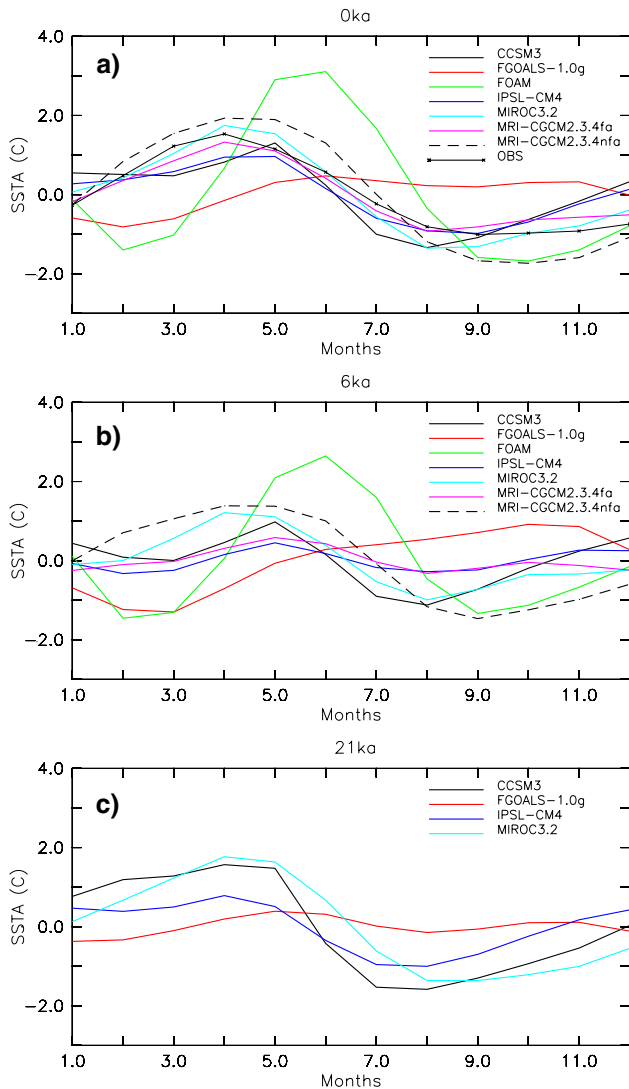
Fig. 4 Seasonal cycles of SSTs (annual mean removed) in the Niño3 region for **a** 0ka; **b** 6ka and **c** 21ka. Each *line* represents a different model and the *solid line with +* in (**a**) stands for NCEP SST observation

annual cycle and semi-annual cycle and the total energy and is computed from a spectral analysis of the full Niño3 monthly SST time series. This diagnosis regards the El Niño as a disruption of the seasonal cycle, a strong seasonal cycle (large SCRS) is less likely to disrupted and vice versa. In the observations, the percentage presents 8.7% of the total energy. In the 0ka simulations, the percentage varies from 0.16% (FGOALS-1.0g) to 51.42% (MRI-CGCM2.3.4nfa). Two models (FGOALS-1.0g, IPSL-CM4) do not have enough energy in the seasonal cycle while three models (FOAM, MIROC3.2, MRI-CGCM2.3.4nfa) have too much energy in the seasonal cycle. Only two models (CCSM3, MRI-CGCM2.3.4fa) have a realistic SCRS. Figure 6d shows that the El Niño amplitude is an inverse function of SCRS like in

observational studies (Gu and Philander 1995; Fedorov and Philander 2001), simple models studies (Chang et al. 1995) and CGCMs (G06).

Following simple ENSO model studies, a "coupling strength" is a measure of the interaction between atmosphere and the ocean. The interannual coupling strength (ICS, G06) is defined as the linear slope of the Gill-type relationship of the wind stress in the Niño4 region and the Niño3 SST anomaly. A stronger slope indicates a larger ICS. Several studies emphasize the roles of the "summer" (June-November) ICS in El Niño growth and amplitude (Zebiak and Cane 1987; Clement et al. 1999). Figure 7 displays the summer ICS calculated for the observations and the PMIP2 simulations. Most models have clearly weaker summer ICS than observations (CCSM3, FGOALS-1.0g, FOAM, IPSL-CM4, MRI-CGCM2.3.4nfa) in the control simulations. Yet the relationship between the El Niño characteristics and the coupling strength as defined in G06 is not conclusive for the PMIP2 models

This analysis of the control simulations show that the PMIP2 set of models shares the same characteristics than models considered in G06. The relationships are more consistent for the El Niño amplitude and are less conclusive for the frequency. Though the PMIP2 models reproduce several basic relationships, they still fail to simulate all the aspects of ENSO variability.

3.2 Changes for MH simulation (mid-Holocene, 6ka BP)

Table 2 shows that the El Niño amplitude of six MH simulations has significantly reduced by 2.9–23% when compared to the control, whereas the El Niño amplitude increase produced by MRI-CGCM2.3.4fa is not statistically significant. This consistent amplitude reduction is in broad agreement with the proxy data (Rodbell et al. 1999). The change of El Niño frequency is less consistent between models and difficult to assess from proxy data, even though five models (FGOALS-1.0g, IPSL-CM4, MIROC3.2 and the two MRIs) have a tendency to produce a lower frequency peak of the Niño3 SST power spectra, with the latter three models also showing a broadening of the power peaks (Fig. 5). One model (CCSM3) shows almost no change of the dominant frequency and the other one (FOAM) changes towards higher frequency.

Compared to the control simulation, all the MH simulations produce annual mean SST cooling in the Niño3 region (not more than 1°C) (Fig. 8a). It is associated with a slight increase of the Niño4 wind stress of most models except for FGOALS-1.0g. There is a slight tendency that models producing the larger also produce the larder increase in easterlies, so that the relationship is in the line
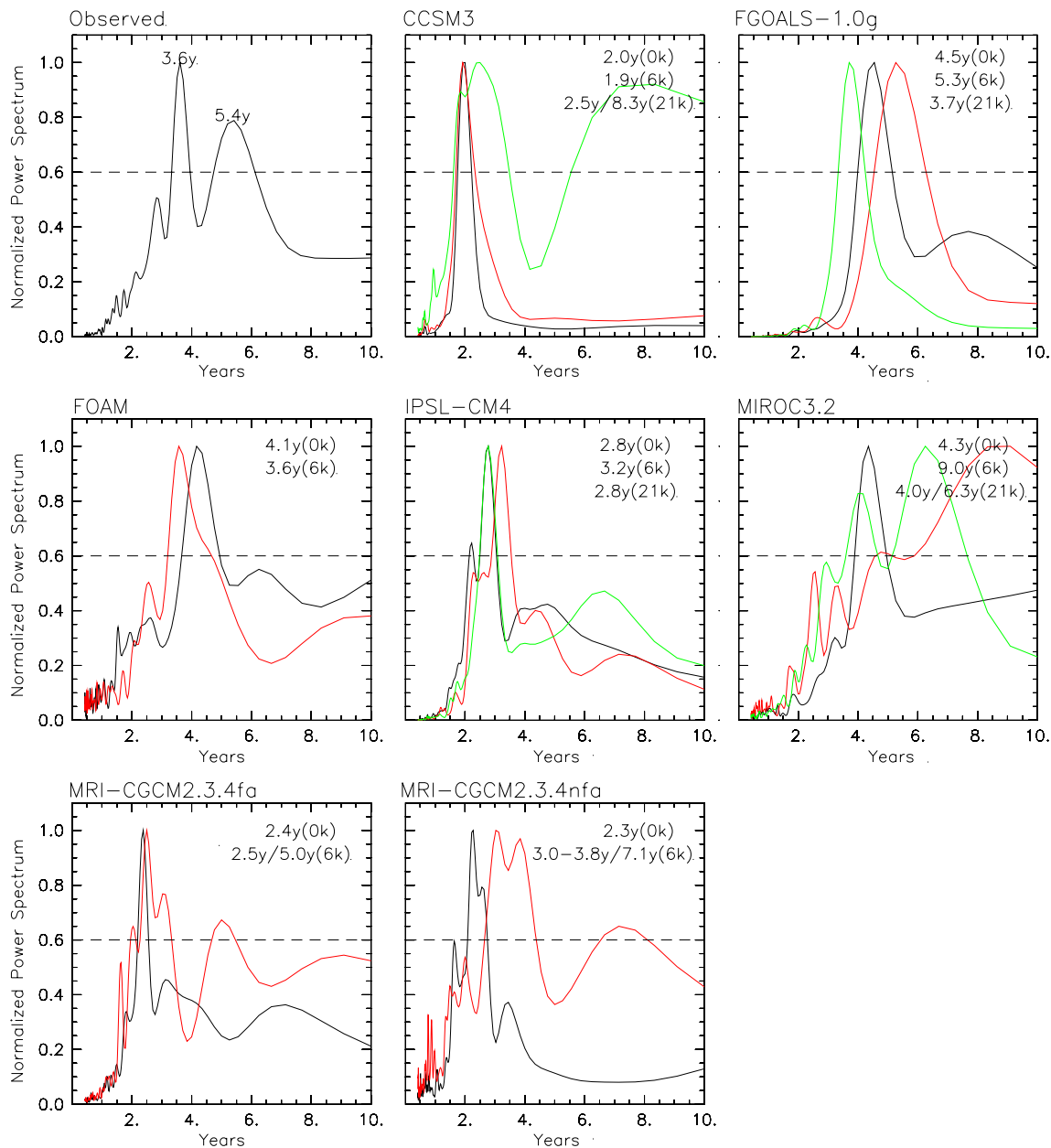
Fig. 5 Normalized power spectra of Niño3 SST anomaly for the seven models studied and the different simulations. Observations are from HadISST1.1 dataset for year 1870–2000. On each graph, the *black line* stands for observations or 0ka, the *red line* for the MH, and the *green line* for the LGM

of the one found across model results for the control simulation (Fig. 8a). However, the SST cooling is of larger scale than just in the eastern Pacific, suggesting that heat fluxes play also a role on the mean state. The relationship found across model results between El Niño amplitude, the Niño4 wind stress, the SPL and the SCRC for the control simulations is found for each of the paleo periods. However, they are not valid when considering the differences between the simulations of the past climates and the control simulations (Fig. 8). For example the reduction of El Niño amplitude is the largest for FGOALS-1.0g for which the

wind stress is reduced. Similarly, FOAM and the two MRIs have nearly the same increase in wind stress but the first two reduce the El Niño amplitude, whereas the flux corrected version of MRI increases it (Fig. 8b).

The decrease in El Niño amplitude of MH is associated with a consistent decrease of the SPL index for most models except for the flux corrected MRI (Fig. 6c). Most models show a decrease of SCRS in the MH simulations while only one model (FGOALS-1.0g) shows a small increase and the reduction of El Niño amplitude would be in factor of increased SCRS. This result suggests that the

Fig. 6 Scatter plot of **a** mean Niño4 τ_x as a function of mean Niño3 SST; **b** El Niño amplitude as a function of mean Niño4 τ_x; **c** El Niño amplitude as a function of the seasonal phase lock, (SPL, see text for definition); **d** El Niño amplitude as a function of the seasonal cycle relative strength. *Black diamonds* stands for 0ka, *red squares* for the MH and *green triangles* for the LGM. The *blue cycle* represents the observations for 1870–2000. The *letters* correspond to model codes as listed in Table 2
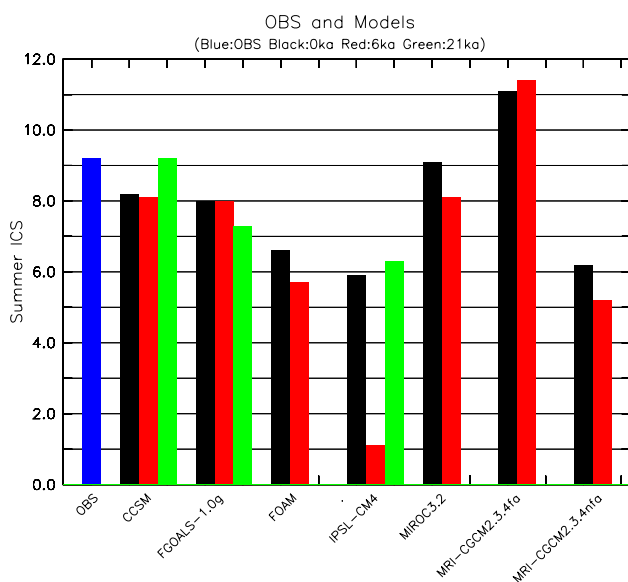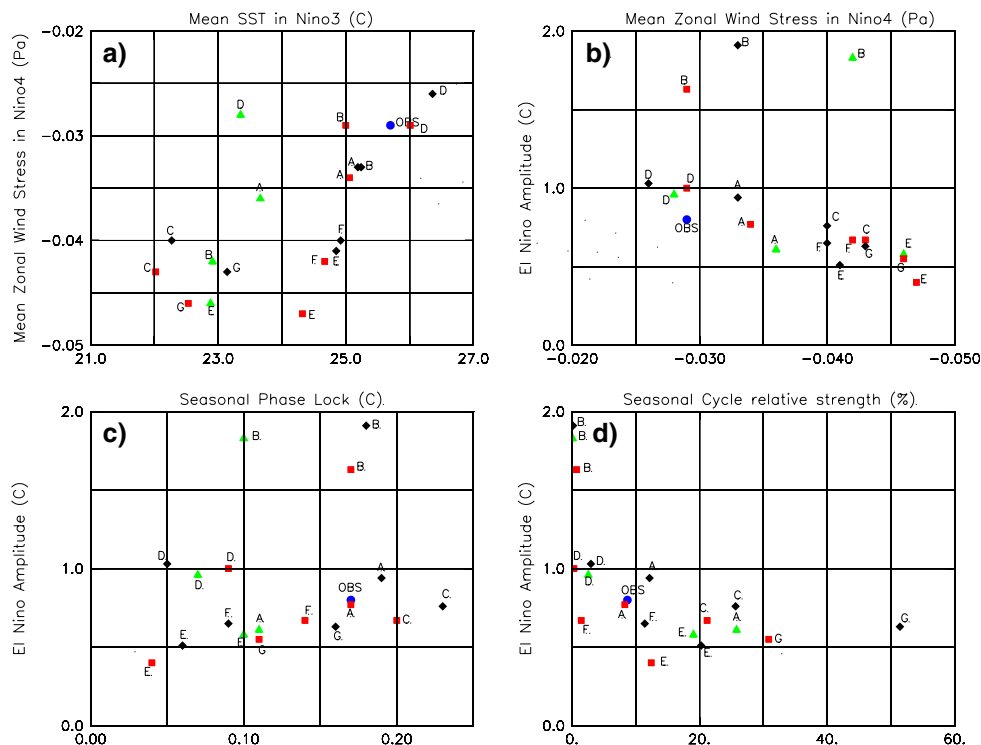
Fig. 7 Summer (June–November) inter-annual coupling strength (SICS) for the observations and the model simulations for 0ka, 6ka and 21ka

reduction of the magnitude of the seasonal cycle is relatively larger than the reduction of the El Niño amplitude and has a large impact on the changes in El Niño characteristics. Considering the coupling strength, most models show a decrease of summer ICS except for the flux-corrected MRI (Fig. 7). Therefore, there is less coupling between the Niño4 wind stress and the Niño3 SST, which

is in good agreement with the reduced El Niño amplitude. The relationship between summer ICS and El Niño frequency is not conclusive.

3.3 Changes for LGM simulation (Last Glacial Maximum, 21ka BP)

In the simulations of LGM, the Niño3 SSTs are lower by −1.6 (CCSM3) to −3°C (IPSL-CM4) colder than in the control simulation while there is only a slight increase of the Niño4 wind stress (Fig. 6a). The relationship between mean SST and wind stress is still found for this time period, but the slope is different. The SST decrease is mainly due to the global cooling caused by the lowered GHG concentrations and the extension of ice sheets (Shin et al. 2003; Braconnot et al. 2007a, b). Three models (CCSM3, FGOALS-1.0g and IPSL-CM4) show a decrease of El Niño amplitude while the other one (MIROC3.2) shows an increase (Table 2, last column). This change is statistically significant only for two models (CCSM3 and MIROC3.2) which exhibit changes of opposite signs. Three models also exhibit a change towards lower frequency and a broadening of the power peaks, even though they are only marginally significant (Fig. 5).

As in the MH, there is no link between the change in El Niño amplitude and the change in wind stress (Fig. 8 b). The linear relationship between El Niño amplitude and SPL follows that of 0ka and the MH simulations except
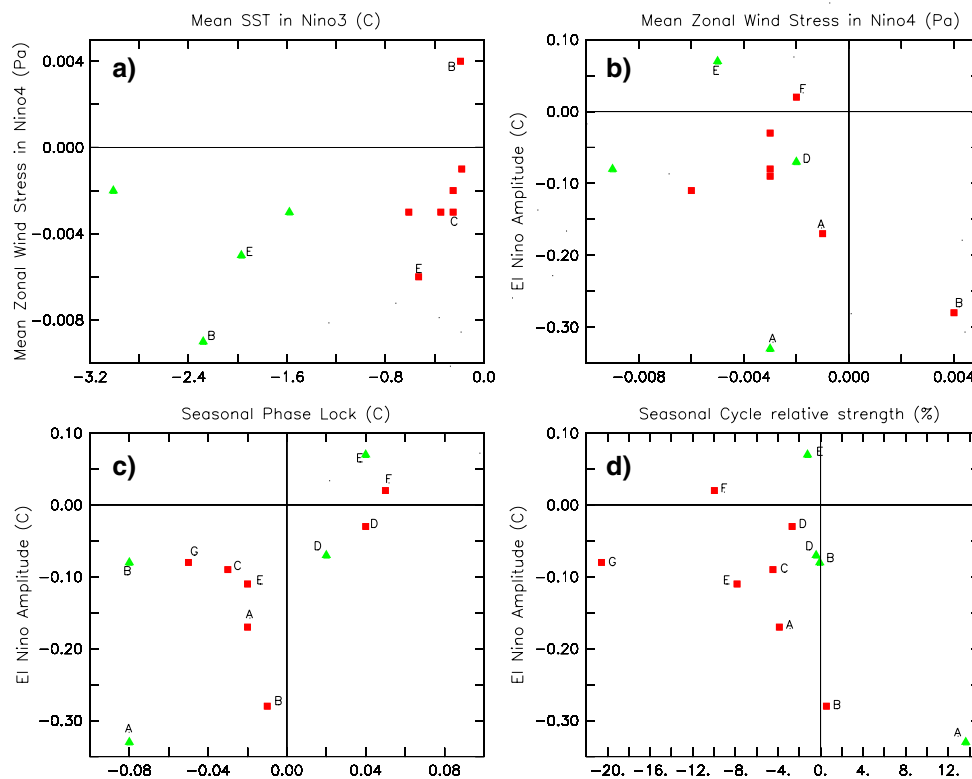
Fig. 8 Scatter plot for the changes between MH (*red squares*) or LGM (*green triangles*) and control simulations of **a** mean Niño4 τ_x as a function of mean Niño3 SST; **b** El Niño amplitude as a function of mean Niño4 τ_x; **c** El Niño amplitude as a function of SPL; **d** El Niño amplitude as a function of SCRS. The *letters* correspond to model codes as listed in Table 2

for IPSL-CM4 (Fig. 6c). When the SPL increases, the El Niño amplitude gets stronger (MRI-CGCM2.3.4fa), whereas other five models show an El Niño amplitude reduction with a decrease of the SPL (Fig. 8c). The SCRS remains nearly as it is in the control simulations, except for CCSM for which it increases by about 14% (Fig. 8d). The seasonal cycle is thus dominant for CCSM3 at LGM, which is consistent with the fact that the seasonal cycle amplitude increases for this model (Fig. 4c) and the El Niño amplitude strongly reduces. The change in summer ICS is model dependent for LGM simulations. Two models (CCSM3 and IPSL-CM4) simulate a small increase of the summer ICS, which in some way is not consistent with the reduced El Niño amplitude for these models. A slight decrease is found for FGOALS-1.0g and no clear slope can be computed for MIROC3 (Fig. 7). Also, the relationship between El Niño dominant frequency and summer ICS is not found across the LGM simulations. The fact that the changes in some of the models do not follow the relationships suggested from theoretical studies or simpler models suggest that changes in the mean state, that are in general not considered in simple analyses, may dominate the changes in ENSO characteristics in some cases.

4 What determines the El Niño changes for MH and LGM?

Several factors can be invoked to explain the El Niño changes found for the MH and LGM and the differences across model results. During an El Niño event, the positive zonal wind stress anomalies would cause a deepening of the eastern equatorial thermocline through the excitation of downwelling Kelvin waves, thus providing a positive feedback for the amplification of the original SST anomaly (Bjerknes 1969). The wind stress anomalies are in a close relationship with the SST gradient which results from the atmosphere–ocean interaction. The response of the atmosphere to SST anomalies is larger in the western part of the Pacific than in the east, which drives an easterly wind anomaly (Clement et al. 2000). The MH El Niño suppression was also attributed to the intensified Asian summer monsoon where the intensified deep convection in the monsoon region increases the Pacific easterly trades through the atmospheric Walker Circulation (Liu et al. 2000). In addition, the signals from subtropical regions also have impacts on the tropical mean thermocline that further influence the ENSO development (Sun and Liu 1996; Clement et al. 1996; Liu et al. 2000).
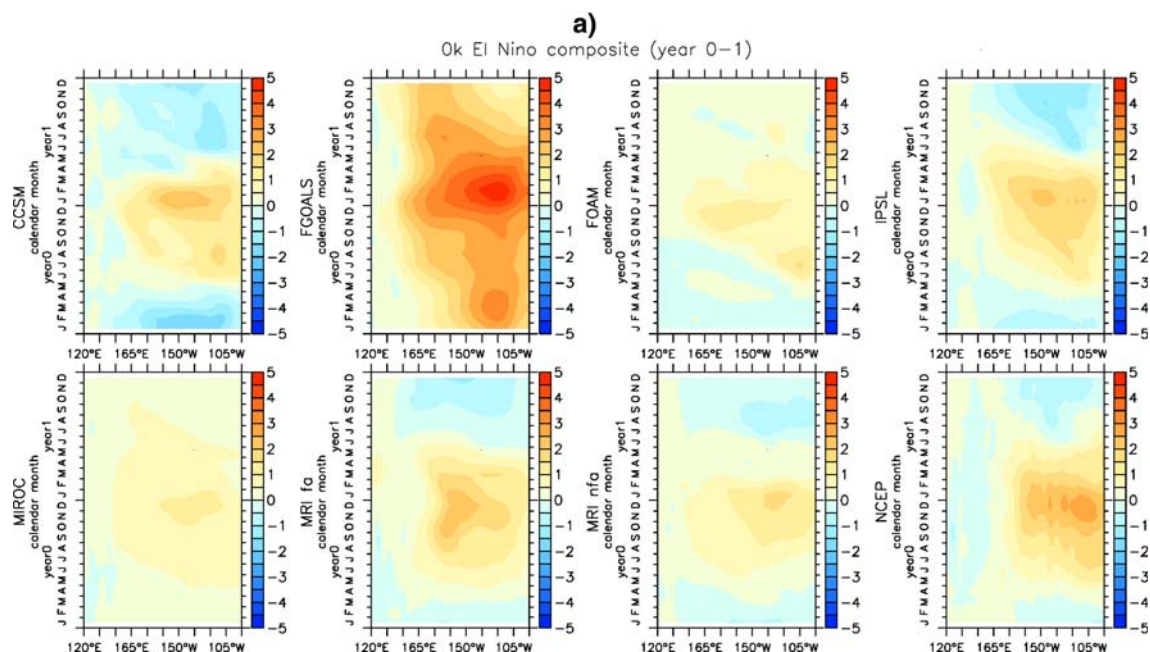
Fig. 9 Time-longitude evolution of the El Niño composite for **a** 0ka; **b** 6ka–0ka; **c** 21ka–0ka, for the year preceding (year 0) and the year following (year 1) an El Niño event. For 0ka isolines are plotted every 0.5°C, whereas for the change at 6ka and at 21ka they are plotted every 0.3°C

In order to analyze the evolution of El Niño events for the different phases of their development, a composite analysis of the equatorial SST is performed. For each model, an individual boreal winter season (DJF) is classified as an El Niño event if the DJF seasonal mean Niño3 SST anomaly exceeds the DJF Niño3 SST standard deviation. The two years (year 0 and year 1) encompassing this El Niño DJF season are analyzed from Hovmoeller diagrams along the equator. The composites of all El Niño events in the control simulations show that the El Niño is locked to the annual cycle with its peak at the end of the calendar year (Fig. 9a). All simulations show anomalous warm SST developing since May–June of year 0 and peaking at the end of the year. Most models also show that the SST anomaly propagates westward across the equatorial Pacific (Fig. 9a). Together with the SST warming in the eastern Pacific, anomalous westerlies gradually develop and the anomalous precipitation increases in the central Pacific (not shown), which is associated to the eastward shift of the Walker circulation.

4.1 Why does the ENSO amplitude reduce in 6ka BP?

The composite analysis shows that the SST anomalies are not as large as in the control simulations from July to December in MH simulations, consistent with the reduction of the El Niño amplitude simulated by most of the models (Fig. 9b). Anomalous precipitation and wind stress are also

reduced (not shown). Analyzing the local amplification of the SST gradient in response to increased solar radiation in boreal summer, the SST gradient between the eastern and western part of the Pacific should be strengthened during the MH, which would favor the anomalous easterlies during autumn and prevent the development of an El Niño (Clement et al. 2000). We investigate this hypothesis by looking at the mean SST change at MH across the equatorial Pacific in autumn. Figure 10a shows that the tendency simulated by all the models would be in favor of a reduction of the SST gradient between 140°E and 100°W (with a warming in the eastern Pacific and a cooling in the central part of the basin). However, most models show an enhancement of the equatorial easterlies in the central and western Pacific (Fig. 10b). Therefore the SST gradient and wind stress feedback is not conclusive for all the models throughout the Pacific basin (Fig. 10). This is also valid for other seasons.

However all models simulate strong easterlies in autumn, which is thus a good candidate for damping the development of El Niño. In the simulations the stronger wind stress is linked to the enhanced summer monsoon and the control of the tropical circulation by the large scale circulation, as discussed by Liu et al. (2000). Indeed, all the coupled models simulate an MH enhancement of monsoon activities during the boreal summer and autumn, though with diverse monsoon behaviors (Fig. 11). This is a direct response to the increased summer insolation in the NH, which strengthens the temperature and pressure contrast
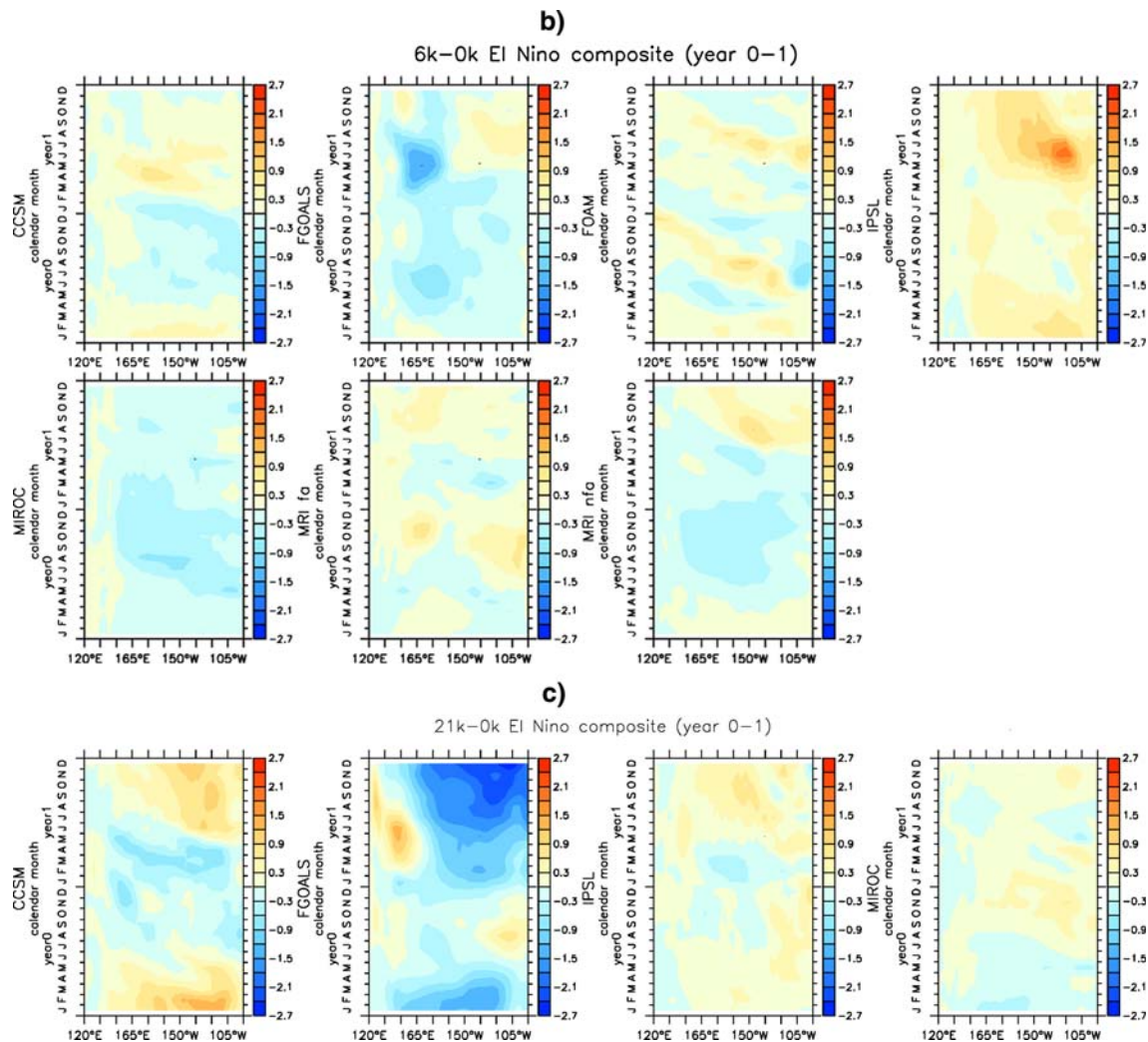
Fig. 9 continued

between the tropical ocean and land and favors the large scale advection of moist air onto the continent where monsoon precipitation develops. The intensified deep convection over the summer monsoon region enhances the atmospheric Walker circulation due to the gear coupling between monsoon circulation and Walker circulation (Wu and Meng 1998) and the regional Hadley circulation in the central Indian Ocean (Goswami et al. 1999). While the Walker circulation is enhanced, the surface easterly anomaly is strengthened and prevents the full development of El Niño. Note also that the strengthening of the easterlies in the middle to the western part of the Pacific in autumn favors a seasonal upwelling over the central to eastern Pacific during the MH (Fig. 12). This upwelling tends to damp the development of the downwelling Kelvin wave associated with the development of an El Niño event. Also all the models simulate a decrease of the seasonal cycle of the Niño3 SST (Fig. 4b). The eastern part of the

basin is warmer in all simulations in the upper ocean layers. Therefore, the weaker vertical temperature gradient during the MH (FOAM, MIROC3.2 and MRInfa-CGCM2.3.4) further weakens the coupling of the subsurface and sea surface and damps the effect of the upwelling temperature anomaly on the SST.

4.2 What are the features for 21ka simulations?

In the LGM simulations, only four models (CCSM3, FGOALS-1.0g, IPSL-CM4 and MIROC3.2) are available in the PMIP2 database and the results show more diversity in simulating the El Niño changes. This is also reflected in the SST composite along the equator during the El Niño year (Fig. 9c). The reduction of the El Niño amplitude simulated by CCSM3, FGOALS and IPSL-CM4 is also characterized by smaller SST anomalies from August of
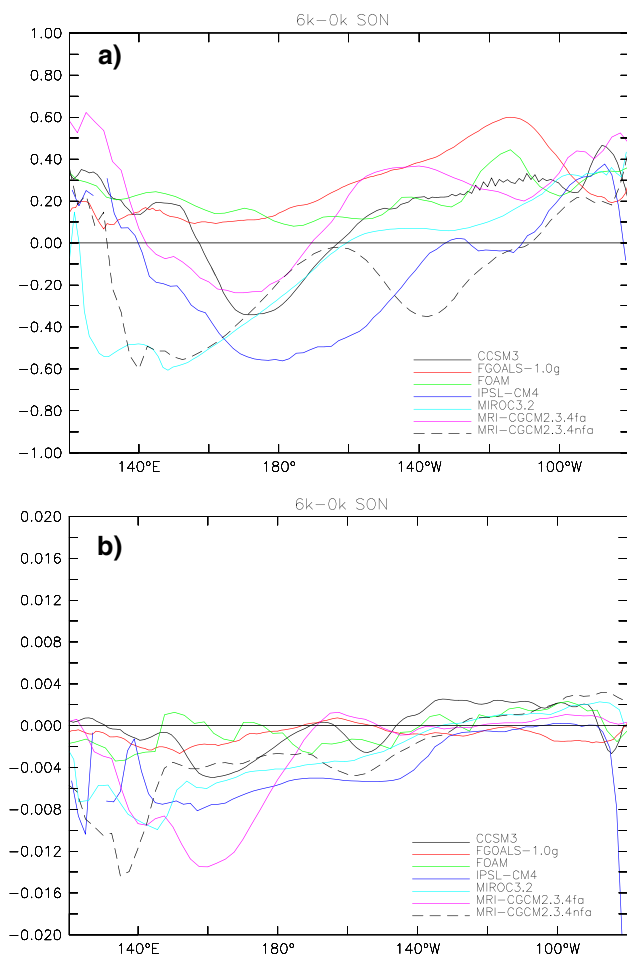
Fig. 10 Change in SST between the MH and the control simulations across the Pacific ocean along the equator. Each *line* represents a different model

the Niño year to August of the following year. Note however that FGOALS and IPSL-CM4 both simulate larger SST anomalies in the eastern part of the basin during the autumn of the Niño year, but that the anomaly does not propagate across the basin. In MIROC3.2, for which El Niño amplitude is increased, a slight increase of the SST anomaly is simulated across the basin, peaking in December in the eastern part of the basin and lasting from the previous August to the following one.

Although all four LGM simulations show a slight increase of the Niño4 wind stress, it doesn't determine the evolution of El Niño as it would be expected from the relationship between wind stress and El Niño amplitude for the control simulations. Indeed, CCSM3 and MIROC 3.2 that produce a statistically significant change in El Niño amplitude, produce changes of opposite sign (Fig. 8b; Table 2). Several differences in their mean state change at LGM could explain these different behaviors. The LGM tropical cooling is rather homogeneous across the Pacific Ocean in CCSM3 (Fig. 3), so that the zonal SST gradient

remains nearly as it is in the pre-industrial experiment. In MIROC3.2 the cooling is larger in the eastern part than in the western part of the basin, and the SST gradient across the basin is enhanced (Fig. 3). The vertical temperature gradient and upwelling changes are also of opposite sign (Fig. 13). These differences may be the reasons for the different El Niño amplitude change.

This analysis shows that the changes in ENSO are less constrained by large scale changes in the equatorial dynamics than for the MH. It also implies that the constraint of the seasonal cycle on the El Niño characteristics is not as strong as in the MH simulations. There is a larger diversity of model response that seems to be dependent on the mean tropical cooling. Heat fluxes and local responses within the Pacific Ocean play a larger role. The coupled models show large diversity in LGM simulations as they do in the future climate projections reported in G06.

5 Conclusions

In this study, we analyzed the changes in the characteristics of El Niño in seven coupled simulations of the MH and four simulations of the LGM. These simulations are part of the coordinated experiments performed as part of the second phase of the PMIP project (Braconnot et al. 2007a). In all our analyses the control simulation is representative of a pre-industrial climate. Overall, the PMIP2 coupled models show more comprehensive details of the atmosphere–ocean coupled system than the AGCM simulations in PMIP1, and offer the possibility to analyze changes in the interannual variability. Most PMIP2 models capture the main features of the present day tropical climate. Several biases are still systematic like too strong mean trade winds, an extensive westward penetration of the equatorial cold tongue and a double ITCZ. Based on the diagnostic methods developed by G06, the relationships between El Niño characteristics and the mean climate of the control simulations are found similar to the results of G06. These models also show their performances in simulating the paleoclimates. The seasonal cycle enlargement of the NH and the summer monsoon system enhancement are well reproduced in the MH simulations. The systematic cooling of the climate system due to the lowered GHG concentrations and the extension of ice sheets in the LGM is also captured.

Although the seasonal cycle of NH is strengthened in the MH, the equatorial Pacific SST amplitude is reduced which implies that the tropical Pacific is not solely determined by the solar radiation but the result of several feedbacks. The composite of El Niño events in the paleoclimate shows little phase locking change of the El Niño evolution with the SST anomaly tending to mature during the boreal winter. However the El Niño amplitude and frequency

Fig. 11 Pattern of sea level pressure change (contour) together with the precipitation change (*shaded*) averaged for JASO months as simulated by the different models. The *lower right corner figure* presents the composite of seven models
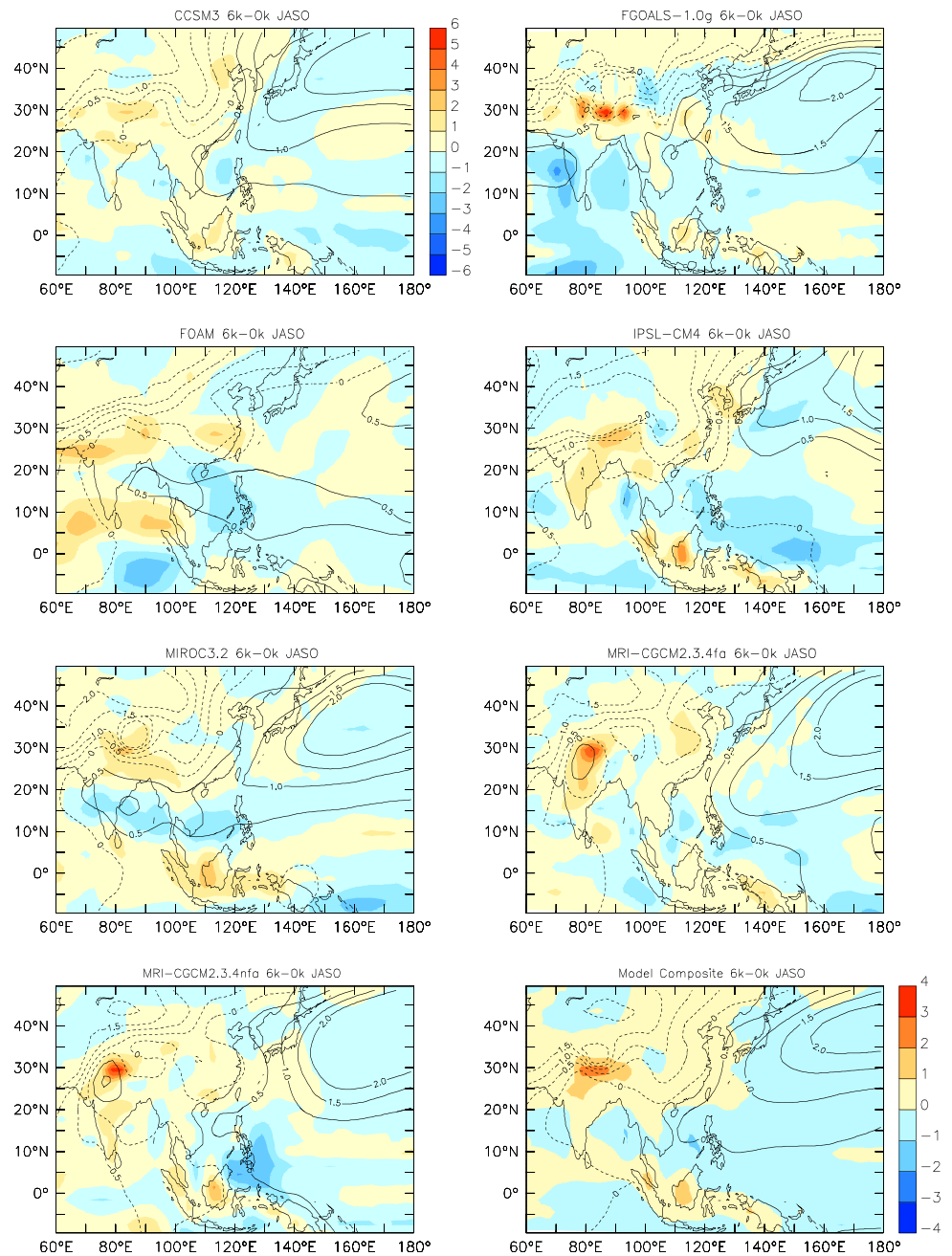
show some significant changes in the paleoclimate. Six out of seven coupled models show that the El Niño events in the MH simulations are significantly damped by 2.9–23%, broadly in agreement with available proxy data (Rodbell et al. 1999). The El Niño amplitude changes in the LGM show more diversity. Also the dominant frequency changes in the MH and LGM are model dependent.

We use the diagnostics used by G06 to analyses El Niño characteristics in simulations of present day climate and in different climate projections where CO_2 is increased by 1% per year until CO_2 doubling and quadrupling. For each scenario similar relationships are found across the different models between the mean state, seasonal cycle and El Niño characteristics. The El Niño amplitude is also shown to be an inverse function of Niño4 mean trade winds. The El Niño amplitude has a linear relation with the seasonal phase locking where a larger SPL provides opportunities for El Niño development. The El Niño amplitude is also shown to be an inverse function of the seasonal cycle relative strength (SCRS). However, what should be noted is that the relationships found for each individual climate state do not apply for the changes between the paleoclimates and the control simulations. This suggests that combinations between changes in the mean state and in

Fig. 12 Longitude-depth pattern of ocean temperature and current difference between the MH (6ka) and the control simulation (0ka), averaged between 2°N and 2°S along the equator in the tropical Pacific
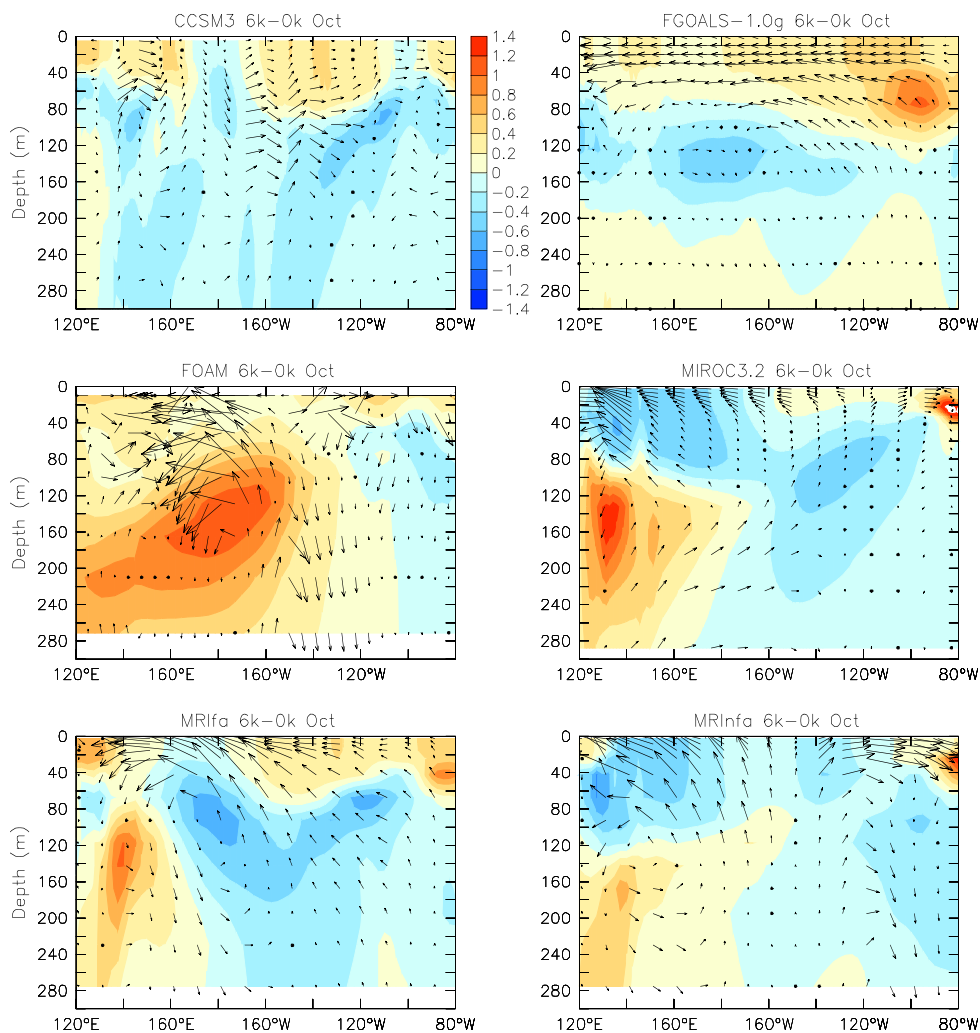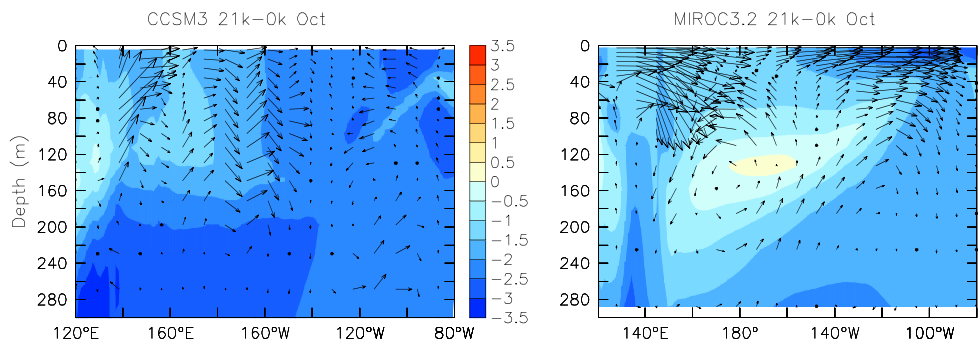

Fig. 13 Same as Fig. 12, but for the difference between the LGM (21ka) and the control simulation (0ka) for CCSM3 and MIROC3.2

climate variability inter into play and modulates the basic El Niño dynamic by altering the coupling between the tropical ocean an the atmosphere, or the characteristics of the equatorial upwelling, both in strength and temperature.

The anomalous easterlies responsible for the El Niño damping in the central to western Pacific are attributed to the asymmetric atmospheric response to the SST gradient along the equatorial Pacific (Clement et al. 2000) or the

enhancement of the Asian summer monsoon system (Liu et al. 2000). We investigate these hypotheses in this study and most coupled models show an easterly enhancement during late summer and autumn which further indicates the important role of the mean wind stress. However, the SST gradient and wind stress feedback is not conclusive for all the models throughout the Pacific basin while all the models simulate the enhancement of the summer monsoon

system. This shows that the large scale circulation changes in the MH play a dominant role in regulating the El Niño amplitude. The mechanism of the relationship between El Niño amplitude and mean climate acts as follows: during the MH simulations, the insolation change caused by the Earth's orbit change result in the enhancement of the seasonal cycle in NH. The enlarged land–sea contrast leads to an enhancement of the summer monsoon system. Due to the coupling interactions between the monsoon circulation and the Walker circulation, anomalous easterlies occur in the central and western Pacific which causes anomalous upwelling in the central and eastern Pacific that suppresses the development of El Niño events. This mechanism is consistent amongst the coupled models and is also consistent with previous results (Liu et al. 2000; Brown et al. 2007). The El Niño amplitude reduction is also related to the weakened seasonal cycle of Niño3 SST and the vertical temperature gradient in the eastern Pacific. This damping of El Niño is certainly at the origin of the reduced teleconnection found by Zhao et al. (2007) between the Pacific Ocean and Sahel precipitation at that time.

The mechanism discussed for the MH does not apply for the LGM simulations. Comparison between two models (CCSM3 and MIROC3.2) suggests that the changes in the mean state have an impact on the El Niño feature change. However the constraint of the seasonal cycle on the El Niño characteristics is not as strong as in the MH simulations. Coupled models show a larger diversity of response to the mean tropical cooling. This result presents some similarities with the results of G06 who show that because of the large inter-model diversity of simulated ENSO, no consistent picture emerges on the future behavior of ENSO. In the case of futures climate changes in the mean state and surfaces fluxes may also be more important than changes in the equatorial dynamics in changing ENSO characteristics. Therefore, the thermodynamical effects in the Pacific Ocean and their roles in regulating ENSO features need to be better understood.

The simple methods used in this study allow us to analyze the basic relationships and mechanisms for each scenario between the El Niño features and the mean states of the tropical Pacific. However, it may have limitations for more comprehensive discussions of the changes between paleoclimates and present day, especially when discussing an individual model's change through the three scenarios. Supposed the relationships are still working, there must be some more dominant mechanisms in determining the El Niño amplitude which needs further discussions. Additionally, the thermocline variations and subtropical impacts may also vary in different climates and should be investigated in future studies.

References

An SI, Timmermann A, Bejarano L, Jin F, Justino F, Liu Z (2004) Modeling evidence for enhanced El Niño-Southern Oscillation amplitude during the Last Glacial Maximum. Paleoceang 19:4009. doi:10.1029/2004PA001020

Battisti DS, Hirst AC (1989) Interannual variability in a tropical atmosphere–ocean model: influence of the basic state, ocean geometry and nonlinearity. J Atmos Sci 46:1687–1712

Berger AL (1978) Long-term variations of caloric insolation resulting from the earth's orbital elements. Q Res 9:139–167

Bjerknes J (1969) Atmospheric teleconnections from the equatorial Pacific. Mon Weather Rev 97:163–172

Braconnot P, Marti O, Joussaume S, Leclainche Y (2000) Ocean Feedback in Response to 6 Kyr BP Insolation. J Clim 13:1537–1553

Braconnot P, Otto-Bleisner BL, Harrison S, Joussaume J, Peterschmitt JY, Abe-Ouchi A, Crucifix M, Fichefet, Hewitt C, Kageyama M, Kitoh A, Laîné A, Loutre MF, Marti O, Merkel U, Ramstein G, Valdes P, Weber L, Yu Y, Zhao Y (2007a) Results of Pmip2 coupled simulations of the mid-Holocene and Last Glacial Maximum—Part 1: Experiments and large-scale features. Clim Past 3(2):261–277

Braconnot P, Otto-Bleisner BL, Harrison S, Joussaume J, Peterschmitt JY, Abe-Ouchi A, Crucifix M, Fichefet, Hewitt C, Kageyama M, Kitoh A, Loutre MF, Marti O, Merkel U, Ramstein G, Valdes P, Weber L, Yu Y, Zhao Y (2007b) Results of Pmip2 coupled simulations of the mid-Holocene and Last Glacial Maximum—Part 2: Feedbacks with emphasis on the location of the ITCZ and mid- and high latitudes heat budget. Climate of the Past 3(2):279–296

Braconnot P, Hourdin F, Bony S, Dufresne JL, Grandpeix JY, Marti O (2007c) Impact of different convective cloud schemes on the simulation of the tropical seasonal cycle in a coupled ocean–atmosphere model. Clim Dyn. doi:10.1007/s00382–007–0244–y

Brown J, Collins M, Tudhope A, Toniazzo T (2007) Modelling mid-Holocene tropical climate and ENSO variability: towards constraining predictions of future change with palaeo-data. Clim. Dyn. doi:10.1007/s00382–007-0270-9

Chang P (1996) The role of the dynamic ocean-atmosphere interactions in tropical seasonal cycle. J Clim 9:2973–2985

Chang P, Ji L, Wang B, Li T (1995) Interaction between the seasonal cycle and El Niño-Southern oscillation in an intermediate coupled ocean–atmosphere model. J Atmos Sci 52:2353–2372

Clement AC, Seager R, Cane MA, Zebiak SE (1996) An ocean dynamical thermostat. J Clim 9:2190–2196

Clement AC, Seager R, Cane MA (1999) Orbital controls on the El Niño/Southern Oscillation and the tropical climate. Paleoceanog 14:441–456

Clement AC, Seager R, Cane MA (2000) Suppression of El Niño during the mid-Holocene by changes in the Earth's orbit. Paleoceanog 15:731–737

Cole J (2001) A slow dance for El Niño. Science 291:1461–1497

Collins WD, Bitz CM, Blackmon ML, Bonan GB, Bretherton CS, Carton JA, Chang P, Doney SC, Hack JJ, Henderson TB, Kiehl JT, Large WG, McKenna DS, Santer BD, Smith RD (2006) The community Climate System Model Version 3 (CCSM3). J Clim 19:2122–2143

Fedorov AV, Philander SG (2001) A stability analysis of tropical ocean–atmosphere interactions: bridging measurements and theory for El Niño. J Clim 14:3086–3101

Gill AE (1982) Atmosphere–Ocean dynamics. Academic, San Diego

Goswami BN, Krishnamurthy V, Annamalai H (1999) A broad-scale circulation index for the interannual variablity of the Indian summer monsoon. Q J R Meteorol Soc 125:611–633

Gu D, Philander SG (1995) Secular changes of annual and inter-annual variability in the tropics during the past century. J Clim 8:864–876

Guilyardi E (2006) El Niño-mean state-seasonal cycle interactions in a multi-model ensemble. Clim Dyn 26:329–348, doi: 10.1007/s00382-005-0084-6

Harrison SP, Braconnot P, Joussaume S, Hewitt C, Stouffer RJ (2002) Fourth international workshop of The Palaeoclimate Modelling Intercomparison Project (PMIP): launching PMIP Phase II. EOS 83:447

Jacob RL, Schafer C, Foster I, Tobis M, Anderson J (2001) Computational Design and performance of the fast ocean-atmosphere model, ver. 1. In: Alexandrov VN, Dongarra JJ, Juliano BA, Renner RS, Tan CJK (eds) Proceedings of the international conference on computational science (ICCS), LNCS 2073. Springer, Heidelberg, pp175–184

Jin FF (1997) An equatorial ocean recharge paradigm for ENSO. Part I: conceptual model. J Atmos Sci 54:811–829

K-1 model developers (2004) K-1 coupled model (MIROC) description. Technical Report 1, Center for Climate System Research, University of Tokyo

Kistler R, Kalnay E, Collins W, Saha S, White G, Woollen J, Chelliah M, Ebisuzaki W, Kanamitsu M, Kousky V, van den Dool H, Jenne R, Fiorino M (2001) The NCEP-NCAR 50-year reanal-ysis: monthly means CD-ROM and documentation. Bull Am Meteorol Soc 82:247–267

Koutavas A, Lynch-Stieglitz J, Marchitto THJ, Sachs JP (2002) El Niño-like pattern in ice age tropical Pacific sea surface temperature. Science 297:226–230

Latif M, Sperber K, Arblaster J, Braconnot P, Chen D, Colman A, Cubasch U, Cooper C, Delecluse P, DeWitt D, Fairhead L, Flato G, Hogan T, Ji M, Kimoto M, Kitoh A, Knutson T, Le Treut H, Li T, Manabe S, Marti O, Mechoso C, Meehl G, Power S, Roeckner E, Sirven J, Terray L, Vintzileos A, Voss R, Wang B, Washington W, Yoshikawa I, Yu J, Zebiak S (2001) Ensip: The El Nino Simulation Intercomparison Project. Clim Dyn 18:255–276

Lea DW, Pak DK, Spero HJ (2000) Climate impact of Late Quaternary equatorial Pacific sea surface temperature variations. Science 289:1719–1724

Liu Z, Kutzbach J, Wu L (2000) Modeling climate shift of El Niño variability in the Holocene. Geophys Res Lett 27:2265–2268

Liu Z, Brady E, Lynch-Steiglitz J (2003) Global ocean response to orbital forcing in the Holocene. Paleoceanograpgy 18(2):1041. doi:10.1029/2002PA00819

Liu ZY, Shin SI, Webb RS, Lewis W, Otto-Bliesner BL (2005) Atmospheric CO$_2$ forcing on glacial thermohaline circulation and climate. Geophys Res Lett 32(2):L02706

Marti O et al (2005) The new IPSL climate system model: IPSL-CM4. Technical report, Institut Pierre Simon Laplace des Sciences de l'Environnement Global IPSL Case101 4 place Jussieu Paris France

Otto-Bliesner BL, Brady EC, Shin SI, Liu Z, Shields C (2003) Modeling El Niño and its tropical teleconnections during the last glacial-interglacial cycle. Geophys Res Lett 30(23):2198. doi: 10.1029/2003GL018553

Peltier WR (2004) Global glacial isostasy and the surface of the ice-age Earth: the ICE-5G (VM2) model and GRACE. Annu Rev Earth Planet Sci 32:111–149. doi: 10.1146/annurev.earth.32.082503.144359

Rasmusson EM, Carpenter TH (1982) Variations in tropical sea surface temperature and surface wind fields associated with the Southern Oscillation/El Niño. Mon Weather Rev 110:354–384

Rayner N, Parker D, Horton E, Folland C, Alexander L, Rowell D, Kent EC, Kaplan A (2003) Global analyses of sea surface temperature, sea ice, and night marine air temperature since the late nineteenth century. J Geophys Res 108:4407. doi: 10.1029/2002JD002670

Rodbell DT, Seltzer GO, Anderson DM, Abbott MB, Enfield DB, Newman JH (1999) An 15000-year record of El Niño-driven alleviation in southwestern Ecuardor. Science 283:1516–1519

Shin SI, Liu Z, B. Otto-Bliesner L, Brady EC, Kutzbach JE, Harrison SP (2003) A simulation of the Last Glacial Maximum Climate using the NCAR CSM. Clim Dyn 20:127–151

Sun DZ, Liu ZY (1996) Dynamic ocean–atmosphere coupling: a thermostat for the tropics. Science 272:1148–1150

Wang C, Picaut J (2004) Understanding ENSO Physics—a review. In: Wang C, Xie SP, Carton JA (eds) Earth's climate: the ocean–atmosphere interaction. Geophysical Monograph Series, AGU, Washington DC, pp 21–48

Wu G, Meng W (1998) Gearing between the Indo-monsoon circulation and Pacific Walker circulation and ENSO I: Data analyses (in Chinese). Chin J Atmos Sci 22:470–480

Yukimoto S, Noda A (2002) Improvements of the Meteorological Research Institute Global Ocean–atmosphere Coupled GCM (MRI-CGCM2) and its climate sensitivity. Tech Report10 NIES Japan

Yu Y, Yu R., Zhang X, Liu H (2002) A flexible global coupled climate model. Adv Atmos Sci 19:169–190

Yu Y, Zhang X, Guo Y (2004) Global coupled ocean–atmosphere general circulation models in LASG/IAP. Adv Atmos Sci 21:444–455

Zebiak SE, Cane MA (1987) A model El Niño-Southern Oscillation. Mon Weather Rev 115:2262–2278

Zhao Y, Braconnot P, Harrison SP, Yiou P, Marti O (2007) Simulated changes in the relationship between tropical ocean temperatures and the western African monsoon during the mid-Holocene. Clim Dyn 28:533–551